Science of the Total Environment 764 (2021) 144607

Contents lists available at ScienceDirect

Science of the Total Environment

journal homepage: www.elsevier.com/locate/scitotenv

# Chemical signature of *Eurois occulta* L. outbreaks in the xylem cell wall of *Salix glauca* L. in Greenland

Angela Luisa Prendin [a,b,*], Marco Carrer [a], Nanna Bjerregaard Pedersen [c], Signe Normand [b,d], Jørgen Hollesen [e], Urs Albert Treier [b,d], Mario Pividori [a], Lisbeth Garbrecht Thygesen [f]

[a] University of Padova, TeSAF Department, Agripolis, Viale dell'Università, 16, 35020 Legnaro, PD, Italy
[b] Aarhus University, Department of Biology, Ecoinformatics and Biodiversity, Ny Munkegade 116, building 1540, 8000 Aarhus C, Denmark
[c] The Royal Danish Academy, Institute of Conservation, Esplanaden 34, 1263 Copenhagen K, Denmark
[d] Center for Biodiversity Dynamics in a Changing World (BIOCHANGE), Department of Biology, Aarhus University, Ny Munkegade 116, building 1540, 8000 Aarhus C, Denmark
[e] The National Museum of Denmark, Environmental Archaeology and Material Science, IC Modewegsvej, Brede, 2800 Kgs. Lyngby, Denmark
[f] University of Copenhagen, Faculty of Science, Department of Geosciences and Natural Resource Management, Rolighedsvej 23, 1958 Frederiksberg C, Denmark

## HIGHLIGHTS

- Insect defoliations cause both plant growth reduction and xylem alteration.
- Under disturbance, lignin and carbohydrate contents changed in fibres, but not in vessels.
- Raman imaging proved useful for studying plant responses to disturbance.

## GRAPHICAL ABSTRACT

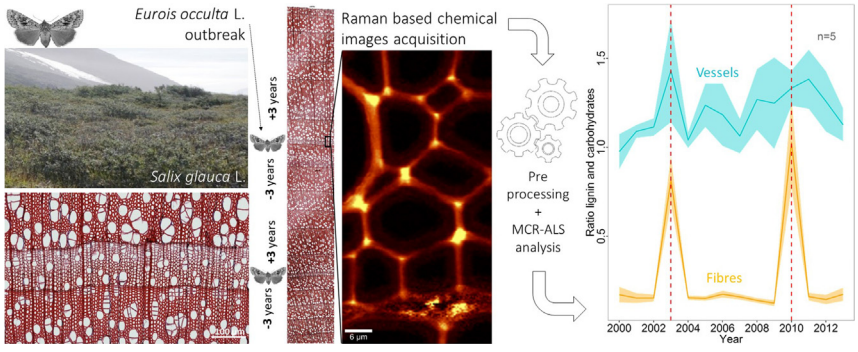


## ARTICLE INFO

*Article history:*
Received 27 February 2020
Received in revised form 29 November 2020
Accepted 17 December 2020
Available online xxxx

Editor: Jose Ignacio Querejeta

*Keywords:*
Chemical imaging
Raman micro-spectroscopy
Insect outbreaks
Lignocellulose
Wood anatomy

## ABSTRACT

Insect defoliations are a major natural disturbance in high-latitude ecosystems and are expected to increase in frequency and severity due to current climatic change. Defoliations cause severe reductions in biomass and carbon investments that affect the functioning and productivity of tundra ecosystems. Here we combined dendro-anatomical analysis with chemical imaging to investigate the direct and lagged effects of insect outbreaks on carbon investment.

We analysed the content of lignin vs. holocellulose, i.e. unspecified carbohydrates in xylem samples of *Salix glauca* L. collected at Iffiartarfik, Nuuk fjord, Greenland, featuring two outbreak events of the moth *Eurois occulta* L. Cross sections of the growth rings corresponding to both outbreaks ±3 years were analysed using confocal Raman imaging to identify possible chemical signatures related to insect defoliation on fibres, vessels, and ray parenchyma cells and to get insight into species-specific defence responses.

Outbreak years with narrower rings and thinner fibre cell walls are accompanied by a change in the content of cell-wall polymers but not their underlying chemistry. Indeed, during the outbreaks the ratio between lignin and carbohydrates significantly increased in fibre but not vessel cell walls due to an increase in lignin content coupled with a reduced content of carbohydrates. Parenchyma cell walls and cell corners did not show any significant changes in the cell-wall biopolymer content.

The selective adjustment of the cell-wall composition of fibres but not vessels under stressful conditions could be related to the plants priority to maintain an efficient hydraulic system rather than mechanical support. However,

* Corresponding author at: University of Padova, TeSAF Department, Agripolis, Viale dell'Università, 16, 35020 Legnaro, PD, Italy.
*E-mail addresses:* angelaluisa.prendin@unipd.it (A.L. Prendin), marco.carrer@unipd.it (M. Carrer), nbje@kglakademi.dk (N. Bjerregaard Pedersen), signe.normand@bios.au.dk (S. Normand), Joergen.Hollesen@natmus.dk (J. Hollesen), urs.treier@bios.au.dk (U.A. Treier), mario.pividori@unipd.it (M. Pividori), lgt@ign.ku.dk (L. Garbrecht Thygesen).

https://doi.org/10.1016/j.scitotenv.2020.144607

the higher lignin content of fibre cell walls formed during the outbreak events could increase mechanical stiffness to the thin walls by optimizing the available resources.
Chemical analysis of xylem traits with Raman imaging is a promising approach to highlight hidden effects of defoliation otherwise overlooked with classical dendroecological methods.


## 1. Introduction

Temperature is one of the major drivers of tundra vegetation as it sets physiological limits to growth (Büntgen et al., 2015; Körner and Paulsen, 2004; Myers-Smith et al., 2015). Nonetheless, climate warming is causing expansion of woody shrub species in the Arctic by relaxing their growth limitations (Elmendorf et al., 2012; Myers-Smith et al., 2011; Myers-Smith and Hik, 2018; Tape et al., 2006). However, not all shrub species within tundra plant assemblages show similar responses. There is evidence that deciduous species benefit more from the improved thermal conditions than evergreen species (DeMarco et al., 2014; Elmendorf et al., 2012; Gough et al., 2012). Yet, such improved growth conditions are not exclusive for plants; insects, including defoliators, also benefit from warming (Huberty and Denno, 2004; Jactel et al., 2012).

Insect defoliations are considered an important co-driver for plant growth and distribution (Dahl et al., 2017; Lund et al., 2017), particularly considering that in the future, insect outbreaks are expected to increase in severity and frequency due to the ongoing warming (Barrio et al., 2017; Callaghan et al., 2004; Chapin et al., 2005). These changes in the disturbance agent regime will likely have cascading consequences for the vegetation biomass and carbon investments, species composition, and for the functioning and productivity of the whole ecosystem (Callaghan et al., 2004; Dahl et al., 2017; Heliasz et al., 2011; López-Blanco et al., 2017; Post and Pedersen, 2008).

In the tundra ecosystem, deciduous species are those most affected by biotic disturbance, notably by insect outbreaks (Lund et al., 2017; Tømmervik et al., 2004; Wilmking et al., 2018; Young et al., 2016). Indeed, recent studies have identified a lack in carbon (C) allocation and primary production in affected shrubs associated to outbreak events (Wilmking et al., 2018; Young et al., 2016). However, rapid regrowth and increased C uptake the following years have also been observed (Dahl et al., 2017; Lund et al., 2017). In particular, the abrupt reduction in ring width observed during the outbreak, seemed compensated by a rapid recovery the following years (Lund et al., 2017). Nevertheless, growth performance should not be the sole metric to assess defoliation effects. When detailed variation in wood anatomy is analysed, in parallel to growth decline, a reduction in the cell-wall thickness can be found and quantified (Wilmking et al., 2018; Young et al., 2016). Therefore, not only growing season temperature (Schweingruber, 1996) but also insect defoliation can influence C allocation to cell-wall thickness (Prendin et al., 2020; Wilmking et al., 2018; Young et al., 2016).

Biotic disturbances result in differences in C allocation to growth, storage, and defence (Moura et al., 2010). Several studies observed that defoliation could also result in modifications of the chemical composition of different organs and tissues, i.e. a reduction of non-structural carbohydrates in needles and stem (Deslauriers et al., 2015) but not in branches (Asshoff and Hattenschwiler, 2006; Handa et al., 2005) and reduced lignin content in the phloem in trees (Villari et al., 2014). Cellulose, hemicellulose, and lignin are the major structural components of the secondary cell wall of wooden cells (Fengel and Wegener, 2003). Lignin provides stiffness and compression strength (Donaldson, 2001) as well as hydrophobicity to cell walls allowing plants to stand upright (Boudet, 2000) supporting water transport (Moura et al., 2010). It also represents a key element in plant defence acting directly as a physical barrier against pathogens (Cabane et al., 2012) and indirectly reducing palatability for herbivores with the increase of leaf toughness and the reduction of nutritional content (War et al., 2012; Johnson et al., 2009). Cellulose provides tensile strength, assuring structural integrity and load bearing capacity to cell walls (Gibson, 2012; Suseela, 2019). In addition, the inter connection between cellulose and hemicellulose in the secondary cell wall (Hayashi, 1989; Bussse-Wicherm et al., 2016) is fundamental in strengthening and relaxing of the cell-wall structure and allows the cells to change shape and size during differentiation (Hayashi and Kaida, 2011). Despite the fact that cell wall biopolymer composition could affect cell and tissue function (Boudet, 2000; Moura et al., 2010), no study has so far investigated the potential alteration in the chemical composition of the walls of different cell types under disturbances. Hence, it is still not clear how the abrupt limitation in C availability due to defoliation could influence the different cell-wall components of the xylem structure and consequently their functionalities. Intense defoliation has been shown to cause not only narrow growth rings but also thinner cell walls, leading to light coloured (white) growth rings. The structure and functionality of these "white rings" (Sutton and Tardif, 2005) could be weakened and reduced due to lower lignin content in the cell wall (Kitin et al., 2010; Voelker et al., 2011). Consequently, this could deteriorate plant defence and favour infestation by pathogens as it happens, for example, with frost damages (Diamandis and Koukos, 1992). In addition, these "white rings" could be more prone to hydraulic failure due to a compromised structure, e.g. micro fractures in the cell wall (Jacobsen et al., 2005). The risk of cavitation during periods of drought the years after defoliation might thus increase (Hillabrand et al., 2019). In general, most research has focused on responses of trees, while to our knowledge, no investigation has been performed on shrubs. Shrubs are one of the key components in tundra vegetation. Gaining knowledge of the possible structural responses that determine species-specific defensive strength and recovery of shrubs could be of high importance for understanding the vegetation dynamics in the tundra. In addition, quantifying those structural adjustments could clarify the role of other factors that, together with increased temperatures (Dahl et al., 2017) or heat-induced drought stress (Parent and Verbyla, 2010), could contribute to a decreased carbon sink capacity of tundra ecosystems.

High resolution chemical imaging techniques permit spatially resolved chemical analysis at cell wall level (Fackler and Thygesen, 2013; Griffith, 2009). Confocal Raman micro-spectroscopy has gained recognition in the fields of wood science and biomass utilization due to the possibility of analysing the biopolymers in situ in the plant cell wall with a high spatial and chemical resolution (Agarwal, 2019; Gierlinger et al., 2012). Raman imaging has previously been used to study the chemical composition of different tissue types, changes in molecular composition, distribution of cell-wall polymers between different cell wall compartments, and cellulose microfibril orientation (Agarwal, 2006; Fredriksson et al., 2018; Gierlinger et al., 2010).

Gray willow (*Salix glauca* L.) is one of the dominant long living deciduous shrub species present in the low Arctic, where it is widespread. It is also one of the most browsed shrubs due to its high leaf palatability and low structural defence (Christie et al., 2015). The noctuid moth *E. occulta* L. is one of the major agents of biotic disturbance of this willow (Karsholt et al., 2015). Intense outbreaks occur under the proper combinations of climatic factors, e.g. temperature, solar radiation, humidity, precipitation, and wind (Vibe, 1971). In this study, we take advantage of a recent dendro-anatomical study on *Salix glauca* L. with samples collected in Iffiartarfik, Nuuk fjord, West Greenland where two outbreak events of the moth *Eurois occulta* L. were identified in 2003 and 2010 (Prendin et al., 2020). Previous results of dendro-anatomical analysis combined with state-of-the art confocal Raman

imaging on the available wood material allow us to shed light on the response strategy of the woody plants under attack. Our aims were to: i) identify the possible differences in biopolymer composition and topological features of cell walls not only between growth years before, under, and after the outbreak events, but also between cell types, i.e. fibres, vessels, ray cells, and cell corners; ii) disentangle the effects of climate and outbreak events on cell-wall biopolymer composition; and iii) understand how possible differences in chemical composition could affect cell functionalities.

## 2. Material and methods

### 2.1. Study area and shrub material

The study area is located in the southern part of West Greenland, at 64°N/50°W along the Nuuk fjord. It is characterized mainly by dry and wet shrub heaths interspersed with dry south-facing slopes and smaller fen areas (Fig. 1 and Fig. S1). The heaths are mainly dominated by *Salix glauca*, *Betula nana,* and *Empetrum nigrum* (Dahl et al., 2017). The Iffiartarfik study site (Fig. S1) is located in the inner part of the fjord system (Fig. 1), which is dominated by warm and dry summers and cold winters (Fenger-Nielsen et al., 2019). Annual mean temperature and total precipitation (1961–1990) in the fjord system are −1.4 °C and 750 mm, respectively (Cappelen et al., 2012). However, in the last decades, an overall warming trend during the growing season (Temperature June–August, T_JJA, data from the regional climate model MAR 3.7 1980-2015) has been recorded in the area (Fig. 1) (Westergaard-Nielsen et al., 2018).

In-situ measurements of soil water content carried out at the study site (Fenger-Nielsen et al., 2019) showed that overall level of soil moisture (from September 2016 to July 2017) in relation to precipitation is well above the threshold for water limitation of arctic shrub growth found by Ackerman et al. (2017). In addition, no clear link is evident between the tasseled cap wetness index (TCW) (Li et al., 2015) and air temperature, precipitation or the drop in NDVI (year 2003 and 2010) (Fig. S2). The drops in NDVI, caused by the almost completely defoliated dwarf shrub vegetation (Lund et al., 2017) allowed for the reconstruction of several outbreak events across the fjord (Prendin et al., 2020).

In total, 24 individuals of *Salix glauca* L. were sampled and used for tree-ring and xylem-trait analysis as described in Prendin et al., 2020. To detect wedging, missing, and false rings, ring width measurements were performed along three to six radii according to stem eccentricity using a LINTAB sliding stage micrometer system (Rinn, Heidelberg, Germany). The obtained measurements were first visually cross-dated, and pointer years of growth suppression during outbreaks of *Eurois occulta* (year 2003 and 2010) were clearly identified together with a significant growth release in the two following years. Then, cross dating accuracy was verified with the computer program COFECHA (Holmes, 1983). A subset of five *S. glauca* individuals was selected and used for Raman image analysis in this study. These five individuals were randomly chosen among 24 shrubs collected at Iffiartarfik in areas that were not limited by soil nutrients (Fenger-Nielsen et al., 2019). The thin sections were selected based on the presence of narrow and evident white rings.

### 2.2. Climate data

Time series of the last 30-y modelled air temperature (3 m above the surface) were obtained from the regional climate model MAR 3.7 (Fettweis et al., 2017) (see Westergaard-Nielsen et al., 2018 for validation of temperatures). Based on these time series, we derived monthly and seasonal variables (e.g. temperature during the growing season June–July-August (T_JJA)).

### 2.3. Sample preparation

Wood discs from the five individuals were soaked in a solution of water and 25% glycerol for three days to soften the tissue. Cross sections (15 μm) were then cut using a rotary microtome (Leica 2245). Glycerol was removed from the microsections by rinsing them in demineralised water. Each wood section was mounted on a microscope slide and covered with a cover glass (thickness n°1, 18 × 18 mm). After gently pressing the cover glass to remove excessive water, samples were semi-permanently fixed with nail polish.

### 2.4. Chemical image acquisition

A full, detailed description of the Raman image acquisition can be found in the Supplementary Information (Table S1). In brief, Raman images were acquired from the cross sections with a confocal Raman microscope (WITec300, WITec GmbH, Ulm, Germany). The width and height of the images were typically in the range from 30 to 50 μm, and the pixel size was 0.3 μm × 0.3 μm. A Raman spectrum was acquired for each pixel. This spectrum provides a molecular "fingerprint" of the chemical composition in that particular location. For each of the five *S. glauca* shrubs, Raman images were acquired for a time span of seven years covering the outbreak year plus the three annual rings

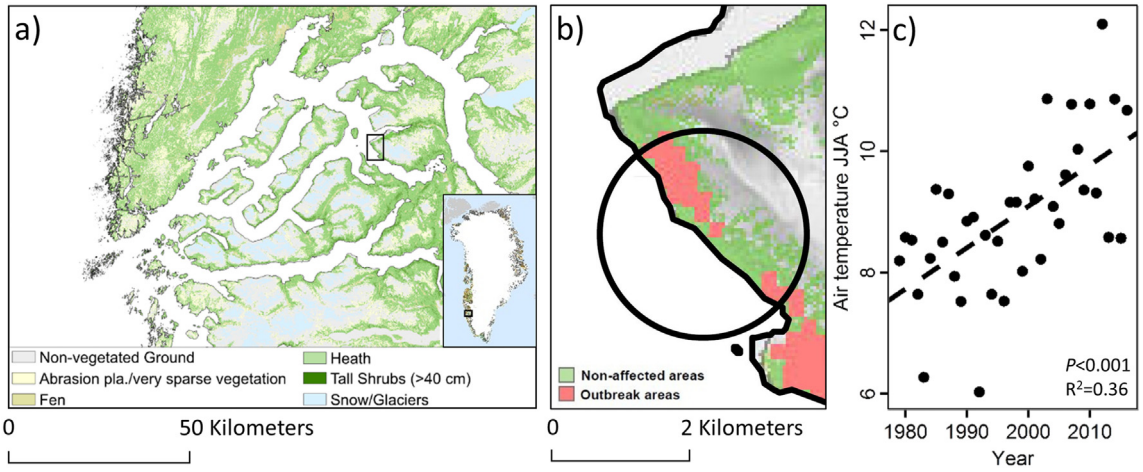


**Fig. 1.** Location and characterization of the study area. a) Vegetation cover map of the Nuuk Fjord in West Greenland (see cropped figure) assessed using a phenology-based approach (Karami et al., 2018). The black square identifies the location of the study site Iffiartarfik. b) Detailed map of the study site showing the areas affected by *Eurois occulta* L. outbreaks (Prendin et al., 2020). c) Growing season (June–July-August) mean temperature from 1980 to 2016 (data from Westergaard-Nielsen et al., 2018).

before and the three years after. This adds up to 70 Raman images in total (two outbreaks × 5 shrubs × 7 years).

### 2.5. Data processing and analysis

A full, detailed description of the data processing and analysis can be found in the Supplementary Information (Table S2), including literature references. In brief, spectra were baseline corrected and the data were visualised as chemical images based on known absorbance bands. From these images, pixels corresponding to specific locations within the tissue were manually selected using the Raman software and a computer mouse. The locations were cell corners, ray parenchyma cell walls, and the second layer (S2) of the secondary cell wall of fibres and vessels.

The data were analysed in four steps. First step was an overview and preliminary check of the selected spectra using Principal Component Analysis (PCA). Second step was Multivariate Curve Resolution – Alternating Least Squares (MCR-ALS) modelling performed on each of the 70 Raman images. This type of modelling deconvolutes the spectra into linear combinations of a few basic spectrum-like components that are the same for all pixels, i.e. only the weights or concentrations of the basic spectra differ between pixels. All models showed the presence of the same four basic components in the Raman spectra: Spectra corresponding to lignin, carbohydrates, water, and noise. Based on this result, it was considered reasonable to combine spectra from all images in common models (step three). Two such common models were prepared: One combined spectra from S2 layers of fibre cell walls, the other from S2 layers of vessel cell walls. An overview of how many spectra were selected from each image is given in Table S3. In the fourth and last step of the analysis, the concentrations of the lignin and carbohydrate components of these two common MCR-ALS models were compared between years by use of Linear Mixed Models (LMM), so that it could be assessed whether differences found were statistically significant.

Linear Mixed Models (LMM) were used to assess the climate-chemistry association and the effects of outbreaks on the time series in both fibres and vessels by using the concentration profiles of the two MCR-ALS multiset model components assigned to carbohydrate and lignin, respectively. Additional models were run excluding the outbreak years to evaluate the climate-chemistry association preventing possible combined effects. The carbohydrate, lignin, and lignin/carbohydrate ratios expressed in the concentration profiles of the multi-set MCR-ALS models were considered as response variables. Monthly or seasonal climate and environmental variables (TCW as indicator of soil moisture availability) were included as fixed effects, and individuals were used as random factors in the initial model (Crawley, 2007). In this way, the LMMs account for variance in the chemical components i) within individuals among years and ii) among individuals growing at the same site. When necessary, response variables were log-transformed to comply with assumptions of normality and homoscedasticity (Zar, 1999; Zuur et al., 2009). The optimal models were selected based on AICc using the maximum likelihood method (Zuur et al., 2009). Finally, we evaluated the fit of the models by graphical examination of the residual and fitted values (Zuur et al., 2009). To evaluate the interference of outbreaks on the climate-chemistry relationship we replicated the LMMs including the categorical factor representing the disturbance events (i.e., the outbreak year plus the three following years of potential recovering) as a fixed effect. The 'lme4' package in R was used to perform these analyses (Bates et al., 2015). The significance of the fixed effects was tested with F-tests (Pinheiro and Bates, 2000) while the conditional $R^2$ was calculated for each model using 'lmerTest' (Kuznetsova et al., 2017).

## 3. Results

### 3.1. Chemical differences between cell compartments and growth years

Average spectra were successfully extracted from all 14 annual rings of the five *Salix glauca* shrubs from the four cell compartments: the cell corners, the S2 layers of fibre and vessel cell walls, and ray parenchyma cells (Fig. 2, Fig. S3 and Fig. S4).

The Raman bands at 1600 $cm^{-1}$ and 1660 $cm^{-1}$ are assigned respectively to aromatic skeletal vibrations and C═C stretching in lignin (Agarwal and Ralph, 2008, 1997). These are very intense in cell corners, present but markedly weaker in S2 layers of fibre cell wall, and of intermediate intensity in S2 layers cell walls of rays and vessels (Fig. 2). In addition, the average Raman spectrum of the cell corners has markedly stronger intensities of bands from 1215 to 1250 and 3000–3070 $cm^{-1}$ assigned to lignin (Larsen and Barsberg, 2010). Relatively stronger bands at 1120, 1150 and between 2930 and 2960 $cm^{-1}$, assigned to holocellulose (Gierlinger and Schwanninger, 2007; Wiley and Atalla, 1987) are observed in the average Raman spectrum of the S2 layer of fibre cell walls compared to the average spectra of the three other cell compartments (Fig. 2).

The differences in chemical composition between the four cell compartments are confirmed by the PCA (Fig. 3). The first principal component (PC1) explains 88% of the variance between spectra. Spectra of cell corners and S2 layer of fibre cell walls fall into two distinct groups, whereas spectra of ray parenchyma and S2 layer of vessel cell walls are placed in overlapping groups among fibres and cell corners. The loading plot of PC1 shows that the intensity of the Raman band at 1600 $cm^{-1}$ assigned to lignin is the major factor explaining the variance between spectra. Hence, the higher the score for PC1, the higher the relative lignin content of the sample. The spectra of ray parenchyma cells and the S2 layer of vessel cell walls are not as clearly separated. However, a clear tendency towards a higher lignin content in S2 layer of vessel cell walls relative to ray parenchyma cells is observed. The second principal component (PC2) explains 7% of the variance between spectra. PC2 shows predominantly positive scores for the S2 layer of fibres cell wall and a mixture of negative and positive scores for cell corners and the S2 layer of vessel cell wall and ray parenchyma cells. The loading plot of PC2 shows that the intensities of the Raman bands at approximately 2900, 1400, 1100 and 380 $cm^{-1}$ primarily explain the differences between the spectra in this direction. Therefore, the explained variance is interpreted as a signal from carbohydrates characterized by higher scores. The carbohydrate content of the S2 layer of fibre cell walls is thereby shown to be relatively higher than that for the three other cell compartments.

The PCA analysis visualizes that the chemical composition of the S2 layer of fibre cell walls in outbreak years is different compared to both the preceding and following years (Fig. 3). All fibres from outbreak years have a higher score for PC1 indicating a higher lignin content relative to carbohydrates. The PCA analysis does not indicate any chemical differences between outbreak and non-outbreak years for the three other cell-wall compartments or shrubs clustering (Fig. S5).

### 3.2. MCR-ALS of individual Raman images

Fig. 4 shows an example of MCR-ALS spectral unmixing of an individual Raman image. The figure includes the pseudo spectra of the four obtained components and a concentration profile showing the location of the individual components in the xylem tissue. All 70 Raman images showed similar results for the same four components. In Fig. 4, the first component shows high band intensity at 1600, 1660, and 3070 $cm^{-1}$ assigned to lignin. In addition, bands with medium to high intensity are present at 1340, 1280, and 1140 $cm^{-1}$ assigned to contributions from both lignin and carbohydrates (Lupoi et al., 2015). The first component is therefore assigned primarily to the lignin polymer of the cell wall. The second component has strong and medium band intensities at 2900, 1410, 1100, 460 and 380 $cm^{-1}$ assigned to contributions from carbohydrate polymers in the cell wall of wood (Lupoi et al., 2015). As for the lignin component, the second component also has medium intensity bands at 1340, 1280, and 1140 $cm^{-1}$ assigned to both lignin and structural carbohydrates in the cell wall. The second component is therefore assigned primarily to structural carbohydrates.

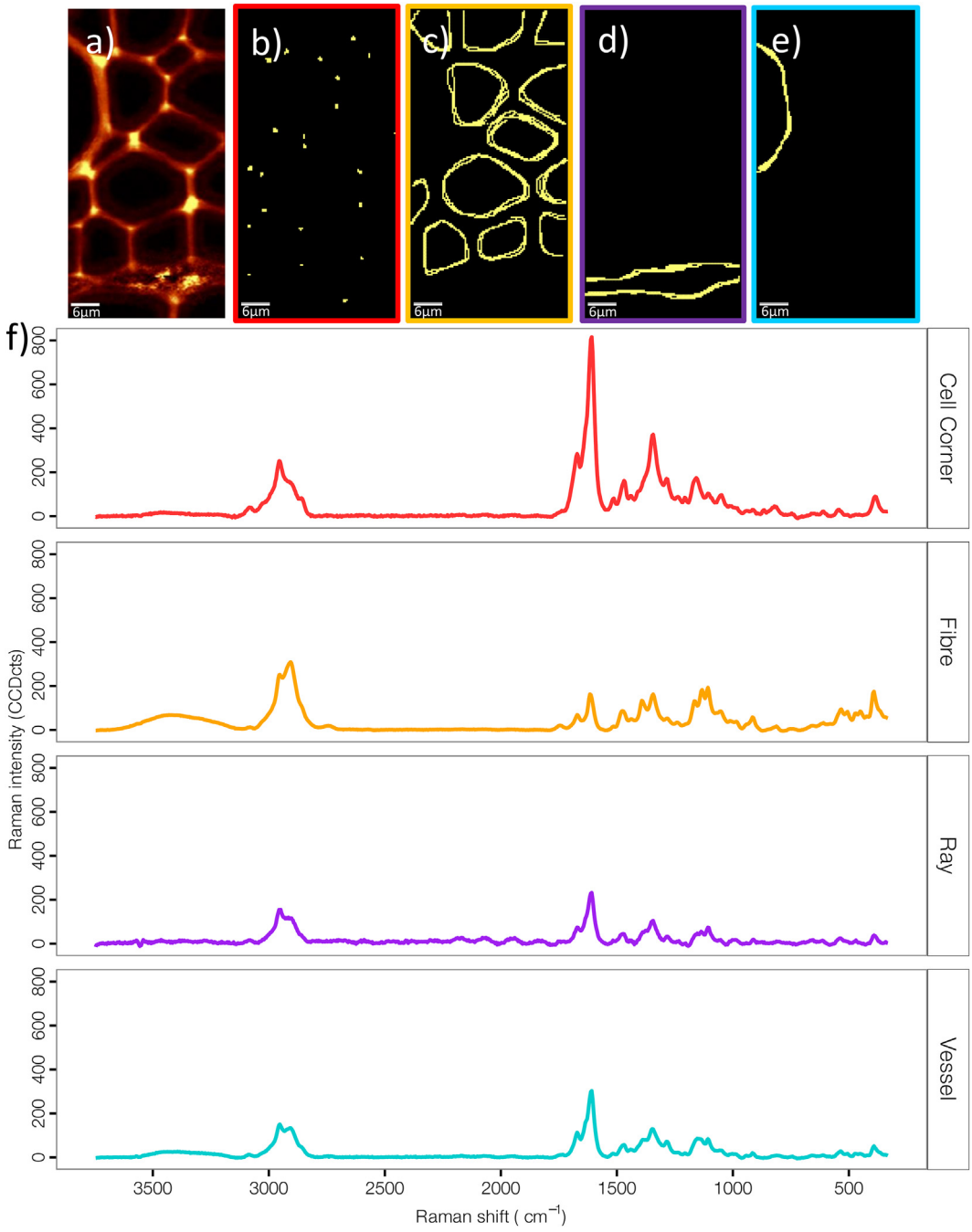


**Fig. 2.** Averaged Raman spectra of the four cell compartments considered in the study. a) Raman image of *Salix glauca* L. cross section generated by using a sum filter around the Raman band at 1600 cm$^{-1}$ assigned to aromatic ring stretching in lignin. b–e) Manual identification of cell corners, and the S2 layer of the secondary cell wall of fibres, vessels, and ray cells at the Raman image to generate average spectra of the four cell wall compartments. The yellow pixels were selected by hand using the Raman software and a computer mouse. f) The obtained average Raman spectra of the four cell compartments shown. The colour code for the frames of panels (b)–(e) is the same as the line colours in panel (f). (For interpretation of the references to colour in this figure legend, the reader is referred to the web version of this article.)

The third component has a broad high intensity band at 3500–3000 cm$^{-1}$ assigned to OH stretching (Wiley and Atalla, 1987), mainly in the lumina. Not showing other intensive constituents, this third component is therefore assigned to water. The fourth and last component has low to medium intensity bands in the whole spectral range. This cannot be assigned to a specific biopolymer and is considered as noise. The intensity of this noise component is higher in the ray (Fig. 4d), which is in agreement with our general observation of higher fluorescence in the ray parenchyma cells during measurements and consequently more noise in these spectra after baseline correction. The carbohydrate and lignin model components were not different, neither between shrubs nor between rings. This points out that the underlying chemistry of the individual biopolymers, as deconvoluted by the MCA analysis, was unaffected by both outbreaks and weather conditions (Fig. S6).

### 3.3. Multiset MCR-ALS of all Raman images

The results of the MCR-ALS models showed that for the individual Raman images, the cell wall biopolymers had the same spectral signatures throughout the data set. Based on these results, selected spectra from all images were combined in two different multiset MCA-ALS models: one based on spectra from the S2 layer of fibre cell walls and

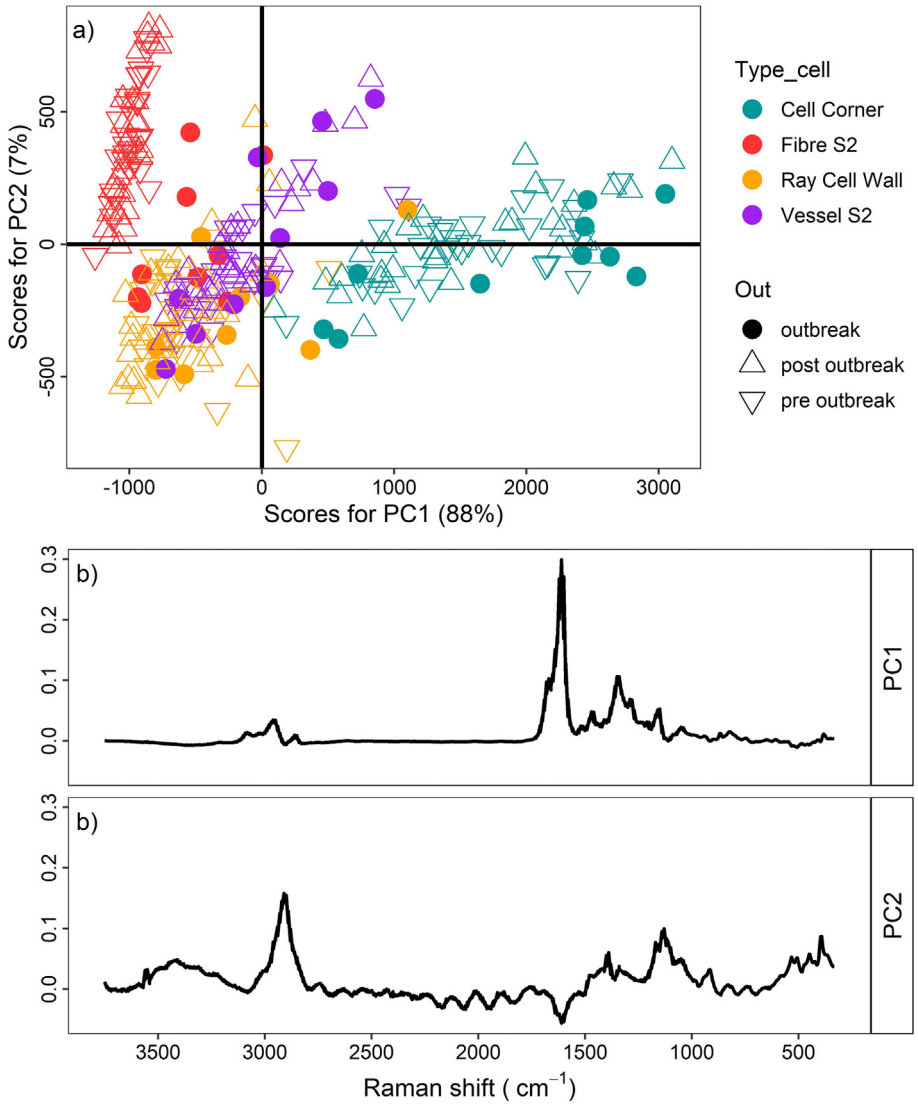


**Fig. 3.** Principal component analysis (PCA) of the chemical composition of the four cell compartments considered in the study. a) Score plot and b) loadings of the first two principal components (PC1 and PC2) of averaged Raman spectra extracted from cell corners and the S2 layer of fibre, ray, and vessel cell walls in 14 annual rings from the five *Salix glauca* individuals. In the score plot the axis labels report the percentage of variance expressed by each component. Colours identify the different cell compartments considered. Closed symbols refer to years characterized by the outbreak events. Open triangles pointing down and open triangles pointing up refer to the three years before and after the outbreak events, respectively.

the other based on spectra from the S2 layer of vessels cell walls. These two models allowed the cell-wall biopolymer contents to be assessed and compared on the same scale within and between Raman images. The average lignin and carbohydrate component concentrations as well as the ratio between these components were calculated for each shrub and for each of the 14 rings (Fig. 5). Considering the period from year 2000 to 2013, lignin and lignin/carbohydrate ratio in fibres and vessels showed a similar trend, with fibres showing lower values compared to vessels. Contrary to this, carbohydrate concentrations were higher in fibres and showed a clear reduction in years 2003 and 2010 corresponding to the outbreak events. In the same years, lignin and lignin/carbohydrate ratio in the fibres showed increased values (Fig. 5). In general, the responses in the outbreak years were stronger in fibres than in vessels for all three components.

### 3.4. LMM of output from multiset MCR-ALS fibre and vessel models

The lignin and carbohydrate pseudo-concentrations shown in Fig. 5 were used for LMM modelling to test for relationships between cell-wall composition, weather conditions, and outbreak years. In the LMM, when including the disturbance factor (the outbreak ± 3 years), the explained variance ($R^2$ conditional) increased from $R^2 = 0.05$ to $R^2 = 0.22$ for the lignin content and slightly decreased from $R^2 = 0.06$ to $R^2 = 0.01$ for the carbohydrate content in the S2 layer of vessel cell walls. The explained variance strongly increased from $R^2 = 0.53$ to $R^2 = 0.81$ in lignin and from $R^2 = 0.16$ to $R^2 = 0.52$ in carbohydrate content in the S2 layer of fibre cell walls (Table 1). As expected, the lignin/carbohydrate ratio was positively related to outbreak events while no relationship was found with the three years following the outbreaks (Table 1).

### 3.5. Outbreaks and climate effects on cell wall chemistry

LMM highlighted that the severe defoliations in 2003 and 2010 affected the content of cell wall polymers. In particular carbohydrates in the fibres were negatively related to outbreaks. The outbreak events had a stronger positive impact on lignin and lignin/carbohydrate ratio in the fibres ($R^2 = 0.81$ and $R^2 = 0.83$) than in the vessels ($R^2 = 0.22$ and $R^2 = 0.25$). In addition, the cell wall chemical composition in fibres and vessels showed a full recovery after the outbreak ($p < .05$). In

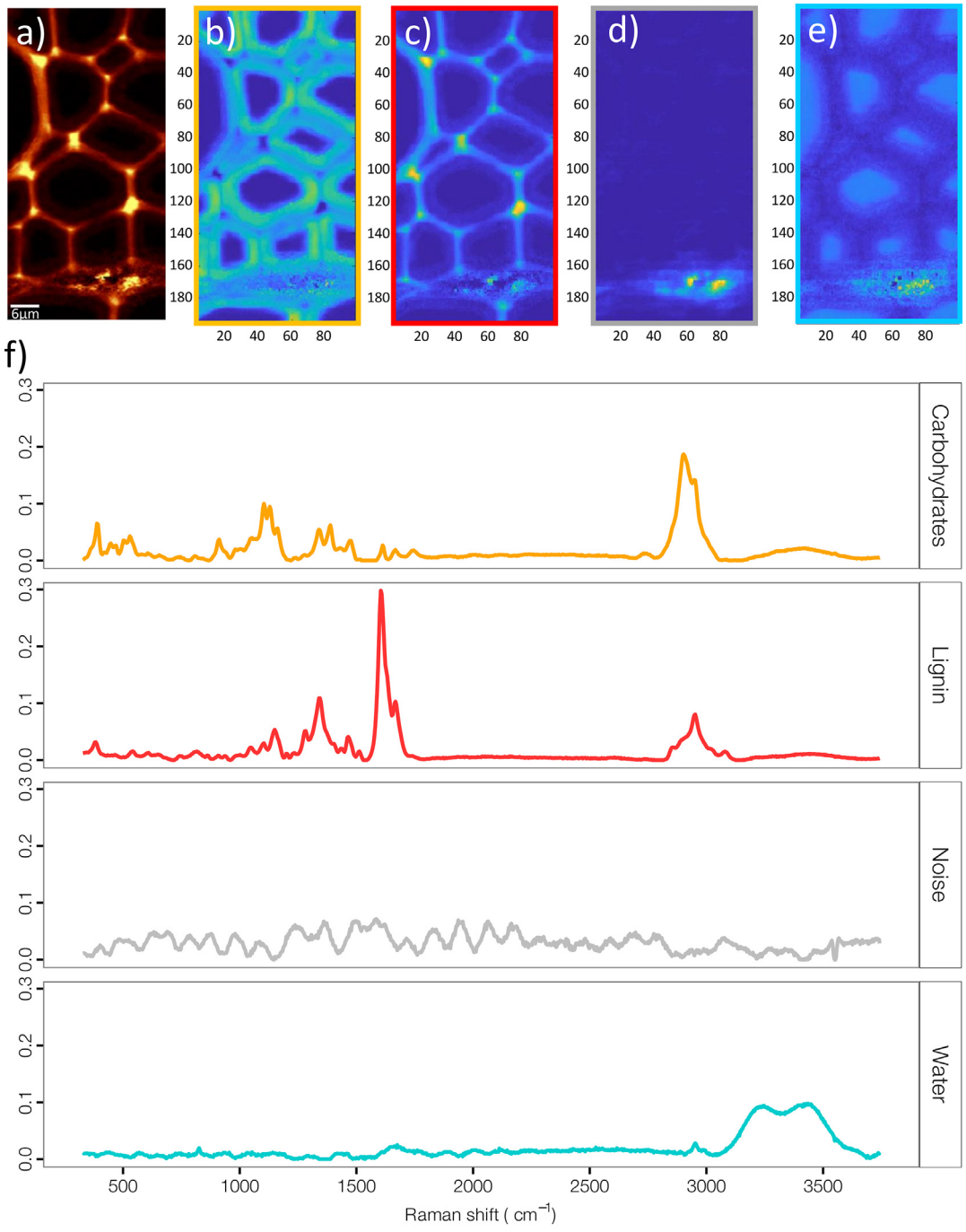


**Fig. 4.** Model components from MCR-ALS single image deconvolution. a) Raman image of *Salix glauca* L. cross section generated as a sum filter around the Raman band at 1600 cm$^{-1}$ assigned to aromatic ring stretching in lignin, i.e. this image is a crude colour-coded representation of lignin concentration, going from black (no lignin) over orange to yellow (high lignin concentration). b–e) MCR-ALS single image deconvolution of the same image as shown in a). The four model components are assigned to carbohydrates, lignin, noise, and water. Concentrations are colour coded in the same way in all four images, going from dark blue (zero) over light blue to yellow (high concentration). f) The obtained basic spectra corresponding to the four model components. The colour code for the frames of panels (b)–(e) is the same as the line colours in panel (f). (For interpretation of the references to colour in this figure legend, the reader is referred to the web version of this article.)

contrast to this result, the temperature of the summer months did not show any significant effect on the chemical composition of fibre and vessel cell walls ($p > .05$) independent of the inclusion/exclusion of the outbreak events (Table 1).

## 4. Discussion

Temperature and biotic disturbances are among the main drivers of vegetation growth in the tundra ecosystems. Defoliations caused by the noctuid moth *E. occulta* L., which represents one of the major agents of biotic disturbance in Greenland, have been documented to be very intense (Karsholt et al., 2015) with marked consequences at ring-width level and xylem structure (Lund et al., 2017; Prendin et al., 2020). Here we show that insect outbreaks can not only cause a drop in the aboveground plant production and cell-wall thickness, but also impact the S2 layer of the xylem cell walls at the chemical level, i.e. the carbohydrate and lignin content. Reduced lignin content in cell walls could have serious structural and functional consequences, such as reduced

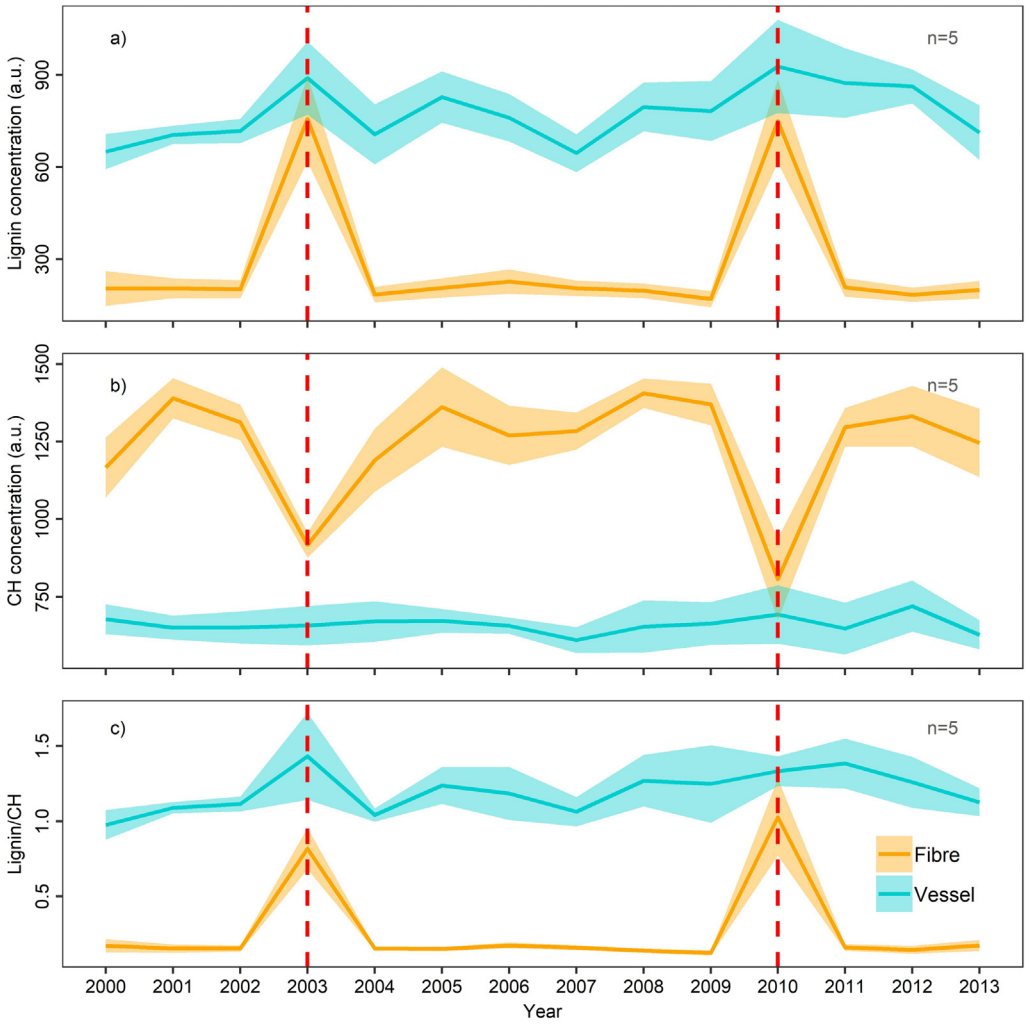


**Fig. 5.** Time series of chemical cell wall components of *Salix glauca* L. from Iffiartarfik in the Nuuk Fjord (West Greenland) based on two multiset MCR-ALS models, one for vessels, one for fibres. The MCR-ALS resolved concentration (arbitrary unit) of lignin, carbohydrates (CH) and their ratios were derived from these two models. Data are means ± SE (Standard Error). Dashed lines indicate the years of the outbreak events.

water conductivity, growth, and survival (Kitin et al., 2010, Voelker et al., 2011).

The observed increase in relative concentration of lignin in the S2 layer of fibre cell walls during outbreak years could represent a shrub response to two different abiotic and biotic drivers: i) a chilling/freezing induced lignin synthesis due to below average growing season temperatures (Cabane et al., 2012); or ii) a plant defence mechanism to leaf browsing that, in Salix spp. during insect attacks, could induce a reduction in leaf area to more than 80% (Boudet, 2000; Moura et al., 2010). Our LMM results point towards this second hypothesis rather than the first, which suggests that even in a temperature-limited environment such as the arctic tundra, biotic disturbances could represent an important driver for the alteration in the chemical composition of the xylem.

### *4.1. Chemical components in different cell compartments*

The average Raman spectra obtained for the four different cell compartments (fibre, vessel, ray parenchyma, and cell corners) show the same characteristic as identified earlier for xylem tissue (Fengel and Wegener, 2003). It is well known that the Raman bands for xylem cell wall biopolymers (i.e. lignin, cellulose, and hemicellulose) overlap with each other but some of the contributions from lignin and carbohydrates are unique (Agarwal and Ralph, 1997; Gierlinger and Schwanninger, 2007). Consequently, we are confident in the correct assignment of PCA loadings as well as MCR-ALS spectral profiles. The Raman bands corresponding to lignin were stronger for cell corners compared to the S2 layer in fibre, vessel, and ray cell walls. Therefore, the shrubs presented high lignin content in cell corners and a much lower relative lignin content in the S2 layer of fibre cell walls, and confirmed earlier results for xylem tissue from other woody species (Fengel and Wegener, 2003; Xu et al., 2006). Additionally, cell corners are considered the starting point for the lignification process (Evert, 2006), where the proportion of lignin decreases from the most external layers of the cell walls to the most internal ones (Rathgeber et al., 2016). Therefore, cell corners together with the middle lamella and the primary wall, being heavily impregnated by the rigid and hydrophobic lignin molecules (Rathgeber et al., 2016) allow xylem cells to be strong, rigid, self-supporting, and waterproof in the external layers, while keeping the inner parts ductile with high tensile strength (Gibson, 2012). The PCA analysis clearly shows a pronounced higher lignin content of the cell corners compared to secondary cell wall of both fibres, rays, and vessels and a lower lignin content of fibre secondary cell walls than secondary cell walls of rays and vessels, confirming what have been previously observed in *Salix gordejecii* trees (Xu et al., 2006). In addition, multiset MCR-ALS analysis combined with LMM modelling showed that fibre cell walls had higher lignin content relative to carbohydrates during the outbreak events. Consequently, we hypothesize that stressful conditions affect the lignification processes to reduce cell

**Table 1**
Results of the optimal linear mixed effect models predicting the climate, e.g. temperature during the growing season (T_JJA), and outbreak effects on cell wall components for the period (2000−2013) and (1980–2016) respectively (see methods for details). In particular, carbohydrates (CH), lignin, and their ratio are considered. Numbers indicate the estimates ± SE (Standard Error). Significant terms are highlighted in bold.

| Model | Response variable | Cell type | T_JJA | Disturbance | | | Intercept | $R^2$ marginal | $R^2$ conditional |
|---|---|---|---|---|---|---|---|---|---|
| | | | | Outbreak | 1 year after | 2 year after | 3 years after | | | |
| Cell wall components | $Log_{10}$(CH) | Vessel | $1.17 \cdot 10^{-3} \cdot \pm 1.23 \cdot 10^{-2}$<br>$5.35 \cdot 10^{-3} \cdot \pm 9.86 \cdot 10^{-3}$ | $7.25 \cdot 10^{-3} \cdot \pm 0.03$ | $1.50 \cdot 10^{-3} \cdot \pm 0.03$ | $0.27 \cdot \pm 0.03$ | $-2.68 \cdot 10^{-3} \cdot \pm 0.03$ | **$2.79 \pm 0.12^{***}$**<br>**$2.76 \pm 0.10^{***}$** | 0.01<br>0.00 | 0.01<br>0.06 |
| | | Fibre | $-1.65 \cdot 10^{-3} \cdot \pm 0.01$<br>$2.79 \cdot 10^{-3} \cdot \pm 7.96 \cdot 10^{-3}$ | **$-0.19 \cdot \pm 0.03^{***}$** | $-0.03 \cdot \pm 0.03$ | $6.36 \cdot 10^{-3} \cdot \pm 0.03$ | $-0.03 \cdot \pm 0.03$ | **$3.13 \pm 1.00^{***}$**<br>**$3.08 \pm 0.08^{***}$** | 0.45<br>0.00 | 0.52<br>0.16 |
| | $Log_{10}$(Lignin) | Vessel | $8.28 \cdot 10^{-4} \cdot \pm 0.01$<br>$8.80 \cdot 10^{-3} \cdot \pm 0.01$ | **$0.09 \cdot \pm 0.04^{*}$** | $0.03 \cdot \pm 0.03$ | $0.07 \cdot \pm 0.04$ | $9.23^{-3} \cdot \pm 0.04$ | **$2.84 \pm 0.14^{***}$**<br>**$2.78 \pm 0.12^{***}$** | 0.11<br>0.01 | 0.22<br>0.05 |
| | | Fibre | $-2.29 \cdot 10^{-3} \cdot \pm 0.02$<br>$-3.98 \cdot 10^{-3} \cdot \pm 0.01$ | **$0.58 \cdot \pm 0.05^{***}$** | $9.08 \cdot 10^{-3} \cdot \pm 0.04$ | $0.01 \cdot \pm 0.04$ | $0.03 \cdot \pm 0.04$ | **$2.29 \pm 0.17^{***}$**<br>**$2.31 \pm 0.15^{***}$** | 0.60<br>0.00 | 0.81<br>0.53 |
| | $Log_{10}$(Lignin/CH) | Vessel | $-2.95 \cdot 10^{-4} \cdot \pm 0.13$<br>$-3.52 \cdot 10^{-3} \cdot \pm 0.01$ | **$0.08 \cdot \pm 0.04^{*}$** | $0.03 \cdot \pm 0.04$ | $0.05 \cdot \pm 0.04$ | $0.01 \cdot \pm 0.04$ | $0.04 \pm 0.13$<br>$0.02 \pm 0.12$ | 0.07<br>0.00 | 0.25<br>0.22 |
| | | Fibre | $-6.54 \cdot 10^{-3} \cdot \pm 0.02$<br>$-6.89 \cdot 10^{-3} \cdot \pm 0.01$ | **$0.78 \cdot \pm 0.05^{***}$** | $0.04 \cdot \pm 0.05$ | $3.54 \cdot 10^{-3} \cdot \pm 0.05$ | $0.06 \cdot \pm 0.05$ | **$-0.85 \pm 0.18^{***}$**<br>**$-0.77 \pm 0.15^{***}$** | 0.74<br>0.00 | 0.83<br>0.44 |

$^{*}p < .05$, $^{**}p < .01$ and $^{***}p < .001$.

expansion and cell wall thickness (Prendin et al., 2020) and to favour the reallocation of carbon resources to other defence mechanism as also observed in trees (Cabane et al., 2012). This could contribute to reduce the impact of pathogens similar to reducing frost damage (Diamandis and Koukos, 1992).

In addition, the individual MCR-ALS models provided nearly identical carbohydrate and lignin components within all shrubs and rings (example shown in Fig. S2). This suggests that the individual biopolymers are chemically similar regardless of individual and yearly variability. Thus, at the level of detail discernible with Raman spectroscopy, lignin produced in outbreak years is not chemically different from lignin produced in other years, indicating its cell compartments to be rather stable and stress resistant.

### 4.2. Time series of cell wall biopolymer content in fibres and vessels

In angiosperm xylem, fibres are mostly devoted to mechanical support, while water transport from root to leaves occurs through the vessels (Hacke, 2015; Myburg et al., 2013). Vessels are intimately connected with living parenchyma cells. This allows for radial transport between tissues and the storage of nonstructural carbohydrates facilitating the exchange of water and solutes between the apoplast and symplast (Hacke, 2015). On the one hand, carbohydrates provide tensile strength while lignin deposited in the middle lamella and the S2 cell wall layer provides compression strength, stiffness (cell wall reinforcement/rigidity), and hydrophobicity facilitating water transport (Boudet, 2000) but also acting as defence agent (Cabane et al., 2012). Therefore, lignin/carbohydrate ratio and lignin composition reflect cell-wall structure and they differ between different positions within the cell wall (Gierlinger, 2014). Our study showed that during the outbreak events, the content of lignin in fibre cell walls increased while the content of carbohydrates decreased. Therefore, the peak in lignin/carbohydrate ratio during outbreak events was caused by adjustment in the content of both these compounds. These results confirm similar structural responses of shrubs and trees. Indeed, under abiotic (Cabane et al., 2012) and biotic disturbances (Bi et al., 2011) lignin synthesis seems to be induced by specific transcription factors that are different from the ones operating in normal years (Cabane et al., 2012). Nevertheless, the increase in lignin and lignin/carbohydrate ratio in the fibres coincides with growth contraction, fibre cell-wall thickness ($CWT_f$), hydraulic diameter, and specific hydraulic conductivity reduction during outbreaks (Prendin et al., 2020). Therefore, under biotic induced C limitation, shrubs tend to maintain an efficient water transport system minimizing the adjustments of the cell-wall components, while the lack in C is reflected in thinner and lignin richer fibre cell walls maximizing mechanical stiffness. In agreement with our results for *S. glauca*, fibre features have also been found to be more sensitive to defoliations than vessel features in another member of the willow family, *Populos tremuloides* Michx., suggesting that the maintenance of an efficient water transport system is frequently prioritized over mechanical support during extreme events (Hillabrand et al., 2019).

### 4.3. Outbreak and climate effects on biochemical composition of wood structure

While willow growth in Iffiartarfik, a typical temperature-limited environment, is significantly correlated to summer air temperature (Prendin et al., 2020), the chemical composition of the willows' woody structure seemed highly independent of this environmental driver. In contrast to previous studies, we found that insect outbreaks have a stronger impact on the chemical composition of xylem cell walls than temperature (Cabane et al., 2012; Hausman et al., 2000), at least during the 14 years period of this study including two insect outbreak events. Considering i) the fundamental increase in the variation explained by the model when we include the outbreak as a categorical factor in the LMMs of the climate–chemical composition association

(Table 1); ii) the better performances of fibre models compared to the vessel models; and iii) the not significant climate–growth relationship obtained even when excluding the outbreak years (Table 1), we can conclude that the *E. occulta* outbreaks are the most likely agent for the increase in lignin content and the decrease in carbohydrate content of fibre cell walls in *S. glauca* in the years 2003 and 2010. The increased lignin content in fibres could potentially mitigate the loss of carbon stored during the outbreak events. Yet, despite the well documented structural recovery the following years (Lund et al., 2017; Prendin et al., 2020), the defoliated shrubs could still be exposed to a higher risk of cavitation in case of a drought event (Hillabrand et al., 2019). Compromised vessels with micro fractures in cell walls or pit membrane overstretching could allow air permeation (Jacobsen et al., 2005). To our knowledge, however, water stress seems unlikely in the area of Iffiartarfik and Nuuk fjord, as soil moisture measurements indicate no water limitation for these sites (Fenger-Nielsen et al., 2019, Hollesen et al., 2019). Nevertheless, this aspect should be considered when studying arctic ecosystems as heat-induced drought stress could increase with ongoing global warming (Parent and Verbyla, 2010; Seo et al., 2015).

## 5. Conclusion

Our study clearly highlights i) that Raman imaging, with the hyper-detailed chemical analysis of individual cell walls and cell-wall layers, allows the detection of chemical signatures of insect outbreaks on different xylem cell types and ii) the high potential in combining dendroecology and spatially resolved biochemical analysis by the use of micro-spectroscopy.

Dendrochemical adjustment of cell-wall composition could identify physiological and anatomical processes driving changes in shrub structure and composition. Moreover, this approach allows to quantify the effect of moth defoliation, not only on shrub woody structure, but at a finer scale such as cell-wall composition. Under stressful conditions, carbon is mostly invested in maintaining water transport efficiency at the cost of adjustments in structure and composition of fibre cell walls. Despite being generally considered a response to either abiotic or biotic stresses to protect plant tissues, in the present case the higher lignin content in fibre cell walls most likely represents a strategy to improve the stiffness of the unusually thin fibre cell walls. This revealed that also in shrubs, the maintenance of an adequate water transport system is prioritized over structural support during extreme events. The weakened structure of fibres could, however, increase the risk of vessel cavitation under potential future drought events in the Arctic. Based on the results of the current study, we expect that Raman microspectroscopy could in the future contribute to improve the understanding of dendroecological inferences especially in understanding plant sink activities, and corresponding adjustments in the carbon budget, lignification, and the possible physiological implications.

## Declaration of competing interest

The authors declare that they have no known competing financial interests or personal relationships that could have appeared to influence the work reported in this paper.

## Acknowledgment

Fieldwork and sampling were carried out as part of the project “Remains of Greenland” with support from VELUX FONDEN (33813). The fieldwork and export permission n° 50.05 were obtained from the Nunatta Katersugaasivia Allagaateqarfialu - Greenland National Museum and Archive. We thank Maria Elena Gelain, Department of Comparative Biomedicine and Food Safety, University of Padua, for providing access to the D-sight 2.0 System automatic scanner used for micro-section imaging and Jakob Johann Assmann for help gathering tasseled cap wetness Index with Google Earth Engine. Confocal Raman imaging collection was carried out by ALP at the Department of Geosciences and Natural Resource Management, University of Copenhagen during a short-term research mission financed by Nordic Forest Research (SNS). ALP was supported by the 2017 BIRD Project of TeSAF Department University of Padova. UAT was supported by the Villum Young Investigator Programme (VKR023456 to SN). NBP was supported by Carlsberg Post doc scholarship (CF14-0454) and Carlsberg Research travel grant (CF15-0112). SN considers this work a contribution to her Sapere Aude Research leader project on “Cross-scale Integration of Arctic Shrub Dynamics” funded by the Independent Research Fund Denmark (7027-00133B). The authors declare no conflicts of interest.

## Funding

This work was supported by: i) 2017 BIRD Project of TeSAF Department University of Padova; ii) Nordic Forest Research (SNS); iii) the Villum Young Investigator Programme (VKR023456 to SN); iv) the Carlsberg Post doc scholarship (CF14-0454); v) Carlsberg Research travel grant (CF15-0112); vi) Independent Research Fund Denmark (7027-00133B); vii) VELUX FONDEN 33813 and viii) partially by Marie Sklodowska-Curie Individual Fellowship (IF) under contract number 895233.

## Authors' contributions

ALP, NBP, SN, MC and LGT planned the research; JH and NBP conducted the fieldwork and collected the plant material. ALP performed laboratory work with the help of NBP and LGT. ALP, NBP, MC and LGT analysed the data. ALP, NBP, MC and LGT wrote the first draft of the manuscript with contributions from UAT and SN. All authors critically revised the manuscript.

## Data availability

The data generated within this study are not public available due to further ongoing studies but can be requested from the corresponding author.

## Appendix A. Supplementary data

Supplementary data to this article can be found online at https://doi.org/10.1016/j.scitotenv.2020.144607.

## References

Ackerman, D., Griffin, D., Hobbie, S.E., Finlay, J.C., 2017. Arctic shrub growth trajectories differ across soil moisture levels. Glob. Chang. Biol. 23, 4294–4302. https://doi.org/10.1111/gcb.13677.

Agarwal, U.P., 2006. Raman imaging to investigate ultrastructure and composition of plant cell walls: distribution of lignin and cellulose in black spruce wood (*Picea mariana*). Planta 224, 1141–1153. https://doi.org/10.1007/s00425-006-0295-z.

Agarwal, U.P., 2019. Analysis of cellulose and lignocellulose materials by raman spectroscopy: a review of the current status. Molecules 24. https://doi.org/10.3390/molecules24091659.

Agarwal, U.P., Ralph, S.A., 1997. FT-Raman spectroscopy of wood: identifying contributions of lignin and carbohydrate polymers in the spectrum of black spruce (*Picea mariana*). Appl. Spectrosc. 51, 1648–1655. https://doi.org/10.1366/0003702971939316.

Agarwal, U.P., Ralph, S.A., 2008. Determination of ethylenic residues in wood and TMP of spruce by FT-Raman spectroscopy. Holzforschung 62, 667–675. https://doi.org/10.1515/HF.2008.112.

Asshoff, R., Hattenschwiler, S., 2006. Changes in needle quality and larch bud moth performance in response to $CO_2$ enrichment and defoliation of treeline larches. Ecol. Entomol. 31, 84–90. https://doi.org/10.1111/j.0307-6946.2006.00756.x.

Barrio, I.C., Rocha, A., Soininen, E.M., Alatalo, J.M., Andersson, T., Buchwal, A., Bueno, C.G., Christie, K.S., Forbes, B.C., Le, E., 2017. Background Invertebrate Herbivory on Dwarf Birch (Betula glandulosa - nana complex) Increases With Temperature and Precipitation Across the Tundra Biome. , pp. 2265–2278 https://doi.org/10.1007/s00300-017-2139-7.

Bates, D., Mächler, M., Bolker, B., Walker, S., 2015. Fitting linear mixed-effects models using lme4. J. Stat. Softw. 67. https://doi.org/10.18637/jss.v067.i01 (arXiv: 1406.5823).

Bi, C., Chen, F., Jackson, L., Gill, B.S., Li, W., 2011. Expression of lignin biosynthetic genes in wheat during development and upon infection by fungal pathogens. Plant Mol. Biol. Report. 29, 149–161. https://doi.org/10.1007/s11105-010-0219-8.

Boudet, A.-M., 2000. Lignins and lignification: selected issues. Plant Physiol. Biochem. 38, 81–96. https://doi.org/10.1016/S0981-9428(00)00166-2.

Büntgen, U., Hellmann, L., Tegel, W., Normand, S., Myers-Smith, I., Kirdyanov, A.V., Nievergelt, D., Schweingruber, F.H., 2015. Temperature-induced recruitment pulses of Arctic dwarf shrub communities. J. Ecol. 103, 489–501. https://doi.org/10.1111/1365-2745.12361.

Bussse-Wicherm, M., Grantham, N.J., Lyczakowski, J.J., Nikolovski, N., Dupree, P., 2016. Xylan decoration patterns and the plant secondary cell wall molecular architecture. Biochem Soc Trans (2016) 44 (1), 74–78. https://doi.org/10.1042/BST20150183.

Cabane, M., Afif, D., Hawkins, S., 2012. Lignins and abiotic stresses, 1st ed. Advances in Botanical Research. Elsevier Ltd. https://doi.org/10.1016/B978-0-12-416023-1.00007-0.

Callaghan, T.V., Björn, L.O., Chernov, Y., Chapin, T., Christensen, T.R., Huntley, B., Ims, R. a, Johansson, M., Jolly, D., Jonasson, S., Matveyeva, N., Panikov, N., Oechel, W., Shaver, G., Elster, J., Henttonen, H., Laine, K., Taulavuori, K., Taulavuori, E., Zöckler, C., 2004. Biodiversity, distributions and adaptations of Arctic species in the context of environmental change. AMBIO A J. Hum. Environ. 33, 404–417. https://doi.org/10.1579/0044-7447-33.7.404.

Cappelen, J., Wang, P.R., Scharling, M., Thomsen, R.S., Boas, L., Vilic, K., Stendel, M., 2012. Danmarks klima 2011 med Tórshavn, Færøerne og Nuuk, Grønland, Teknisk rapport 12–01. Danish Meteorological Institute, Copenhagen (in Danish, English summary).

Chapin, I.I.I.F.S., Sturm, M., Serreze, M.C., McFadden, J.P., Key, J.R., Lloyd, A.H., McGuire, A.D., Rupp, T.S., Lynch, A.H., Schimel, J.P., Beringer, J., Chapman, W.L., Epstein, H.E., Euskirchen, E.S., Hinzman, L.D., Jia, G., Ping, C.-L., Tape, K.D., Thompson, C.D.C., Walker, D.A., Welker, J.M., 2005. Role of land-surface changes in Arctic summer warming. Science 310 (5748), 657–660. https://doi.org/10.1126/science.1117368.

Christie, K.S., Bryant, J.P., Gough, L., Ravolainen, V.T., Ruess, R.W., Tape, K.D., 2015. The role of vertebrate herbivores in regulating shrub expansion in the Arctic: a synthesis. Bioscience 65, 1123–1133. https://doi.org/10.1093/biosci/biv137.

Crawley, M.J., 2007. Mixed-effects models. R Book, Second edition, pp. 681–714.

Dahl, M.B., Priemé, A., Brejnrod, A., Brusvang, P., Lund, M., Nymand, J., Kramshøj, M., Ro-Poulsen, H., Haugwitz, M.S., 2017. Warming, shading and a moth outbreak reduce tundra carbon sink strength dramatically by changing plant cover and soil microbial activity. Sci. Rep. 7, 1–13. https://doi.org/10.1038/s41598-017-16007-y.

DeMarco, J., MacK, M.C., Bret-Harte, M.S., Burton, M., Shaver, G.R., 2014. Long-term experimental warming and nutrient additions increase productivity in tall deciduous shrub tundra. Ecosphere 5, 1–22. https://doi.org/10.1890/ES13-00281.1.

Deslauriers, A., Caron, L., Rossi, S., 2015. Carbon allocation during defoliation: testing a defense-growth trade-off in balsam fir. Front. Plant Sci. 6, 1–13. https://doi.org/10.3389/fpls.2015.00338.

Diamandis, S., Koukos, P., 1992. Effect of bacteria on the mechanical and chemical properties of wood in poplars damaged by frost cracks. For. Pathol. 22, 362–370. https://doi.org/10.1111/j.1439-0329.1992.tb00308.x.

Donaldson, L.A., 2001. Lignification and lignin topochemistry - an ultrastructural view. Phytochemistry 57, 859–873. https://doi.org/10.1016/S0031-9422(01)00049-8.

Elmendorf, S.C., Henry, G.H.R., Hollister, R.D., Björk, R.G., Bjorkman, A.D., Callaghan, T.V., Collier, L.S., Cooper, E.J., Cornelissen, J.H.C., Day, T.A., Fosaa, A.M., Gould, W.A., Grétarsdóttir, J., Harte, J., Hermanutz, L., Hik, D.S., Hofgaard, A., Jarrad, F., Jónsdóttir, I.S., Keuper, F., Klanderud, K., Klein, J.A., Koh, S., Kudo, G., Lang, S.I., Loewen, V., May, J.L., Mercado, J., Michelsen, A., Molau, U., Myers-Smith, I.H., Oberbauer, S.F., Pieper, S., Post, E., Rixen, C., Robinson, C.H., Schmidt, N.M., Shaver, G.R., Stenström, A., Tolvanen, A., Totland, Ø., Troxler, T., Wahren, C.-H., Webber, P.J., Welker, J.M., Wookey, P.A., 2012. Global assessment of experimental climate warming on tundra vegetation: heterogeneity over space and time. Ecol. Lett. 15, 164–175. https://doi.org/10.1111/j.1461-0248.2011.01716.x.

Evert, R.F., 2006. Esau's Plant Anatomy, Meristems, Cells, and Tissues of the Plant Body: Their Structure, Function, and Development. 3rd edn. John Wiley & Sons, Inc., Hoboken, NJ, USA https://doi.org/10.1002/0470047380.

Fackler, K., Thygesen, L.G., 2013. Microspectroscopy as applied to the study of wood molecular structure. Wood Sci. Technol. 47, 203–222. https://doi.org/10.1007/s00226-012-0516-5.

Fengel, D., Wegener, G., 2003. Wood. Chemistry, Ultrastructure, Reactions. Kessel Verlag, Remangen.

Fenger-Nielsen, R., Hollesen, J., Matthiesen, H., Andersen, E.A.S., Westergaard-Nielsen, A., Harmsen, H., Michelsen, A., Elberling, B., 2019. Footprints from the past: the influence of past human activities on vegetation and soil across five archaeological sites in Greenland. Sci. Total Environ. 654, 895–905. https://doi.org/10.1016/j.scitotenv.2018.11.018.

Fettweis, X., Box, J.E., Agosta, C., Amory, C., Kittel, C., Lang, C., Van As, D., Machguth, H., Gallée, H., 2017. Reconstructions of the 1900-2015 Greenland ice sheet surface mass balance using the regional climate MAR model. Cryosphere 11, 1015–1033. https://doi.org/10.5194/tc-11-1015-2017.

Fredriksson, M., Pedersen, N.B., Thygesen, L.G., 2018. The cell wall composition of Norway spruce earlywood and latewood revisited. Int. Wood Prod. J. 9, 80–85. https://doi.org/10.1080/20426445.2018.1479680.

Gibson, L.J., 2012. The hierarchical structure and mechanics of plant materials. J. R. Soc. Interface 9, 2749–2766. https://doi.org/10.1098/rsif.2012.0341.

Gierlinger, N., 2014. Revealing changes in molecular composition of plant cell walls on the micron-level by Raman mapping and vertex component analysis (VCA). Front. Plant Sci. 5. https://doi.org/10.3389/fpls.2014.00306.

Gierlinger, N., Schwanninger, M., 2007. The potential of Raman microscopy and Raman imaging in plant research. Spectroscopy 21, 69–89. https://doi.org/10.1155/2007/498206.

Gierlinger, N., Luss, S., Konig, C., Konnerth, J., Eder, M., Fratzl, P., 2010. Cellulose microfibril orientation of *Picea abies* and its variability at the micron-level determined by Raman imaging. J. Exp. Bot. 61, 587–595. https://doi.org/10.1093/jxb/erp325.

Gierlinger, N., Keplinger, T., Harrington, M., 2012. Imaging of plant cell walls by confocal Raman microscopy. Nat. Protoc. 7, 1694–1708. https://doi.org/10.1038/nprot.2012.092.

Gough, L., Moore, J.C., Shaver, G.R., Simpson, R.T., Johnson, D.R., 2012. Above- and belowground responses of arctic tundra ecosystems to altered soil nutrients and mammalian herbivory. Ecology 93, 1683–1694. https://doi.org/10.1890/11-1631.1.

Griffith, P.R., 2009. Infrared and Raman Instrumentation for Mapping and Imaging in Infrared and Raman Spectroscophy Imaging. Wiley-VCH.

Hacke, U., 2015. Functional and Ecological Xylem Anatomy. Springer International Publishing, Cham https://doi.org/10.1007/978-3-319-15783-2.

Handa, I.T., Körner, C., Hättenschwiler, S., 2005. A test of the treeline carbon limitation hypotesis by in situ $CO_2$ enrichment and defoliation. Ecol. Funct. 86, 1288–1300.

Hausman, J.F., Evers, D., Thiellement, H., Jouve, L., 2000. Compared responses of poplar cuttings and in vitro raised shoots to short-term chilling treatments. Plant Cell Rep. 19, 954–960. https://doi.org/10.1007/s002990000229.

Hayashi, T., 1989. Xyloglucans in the primary cell wall. Annu. Rev. Plant Physiol. Plant Mol. Biol. 40, 139–168. https://doi.org/10.1146/annurev.pp.40.060189.001035.

Hayashi, T., Kaida, R., 2011. Functions of xyloglucan in plant cells. Mol. Plant 4, 17–24. https://doi.org/10.1093/mp/ssq063.

Heliasz, M., Johansson, T., Lindroth, A., Mölder, M., Mastepanov, M., Friborg, T., Callaghan, T.V., Christensen, T.R., 2011. Quantification of C uptake in subarctic birch forest after setback by an extreme insect outbreak. Geophys. Res. Lett. 38. https://doi.org/10.1029/2010GL044733 n/a-n/a.

Hillabrand, R.M., Lieffers, V.J., Hogg, E.H., Martínez-Sancho, E., Menzel, A., Hacke, U.G., 2019. Functional xylem anatomy of aspen exhibits greater change due to insect defoliation than to drought. Tree Physiol. 39, 45–54. https://doi.org/10.1093/treephys/tpy075.

Hollesen, J., Matthiesen, H., Fenger-Nielsen, R., Abermann, J., Westergaard-Nielsen, A., Elberling, B., 2019. Predicting the loss of organic archaeological deposits at a regional scale in Greenland. Scientific Reports 9 (1), 9097. https://doi.org/10.1038/s41598-019-45200-4.

Holmes, R.L., 1983. Computer-assisted quality control in tree-ring dating and measurement. Tree-Ring Bull. 43, 69–78.

Huberty, A.F., Denno, R.F., 2004. Plant water stress and its consequences for herbivorous insects: a new syntesis. Ecology 85, 1383–1398. https://doi.org/10.1890/03-0352.

Jacobsen, A.L., Ewers, F.W., Pratt, R.B., Paddock, W.A., Davis, S.D., 2005. Do xylem fibers affect vessel cavitation resistance? Plant Physiol. 139, 546–556.

Jactel, H., Petit, J., Desprez-Loustau, M.L., Delzon, S., Piou, D., Battisti, A., Koricheva, J., 2012. Drought effects on damage by forest insects and pathogens: a meta-analysis. Glob. Chang. Biol. 18, 267–276. https://doi.org/10.1111/j.1365-2486.2011.02512.x.

Johnson, M.T.J., Smith, S.D., Rausher, M.D., 2009. Plant sex and the evolution of plant defenses against herbivores. Proc. Natl. Acad. Sci. U. S. A. 106, 18079–18084 (PMID: 19617572). https://doi.org/10.1073/pnas.0904695106.

Karami, M., Westergaard-Nielsen, A., Normand, S., Treier, U.A., Elberling, B., Hansen, B.U., 2018. A phenology-based approach to the classification of Arctic tundra ecosystems in Greenland. ISPRS J. Photogramm. Remote Sens. 146, 518–529. https://doi.org/10.1016/j.isprsjprs. 2018.11.005.

Karsholt, O., Kristensen, N.P., Simonsen, T.J., Ahola, Matti, 2015. *Lepidoptera* (moths and butterflies). The Greenland Entomofauna: An Identification Manual of Insects, Spiders and their Allies, pp. 302–352.

Kitin, P., Voelker, S.L., Meinzer, F.C., Beeckman, H., Strauss, S.H., Lachenbruch, B., 2010. Tyloses and phenolic deposits in xylem vessels impede water transport in low-lignin transgenic poplars: a study by cryo-fluorescence microscopy. Plant Physiol. 154, 887–898. https://doi.org/10.1104/pp.110.156224.

Körner, C., Paulsen, J., 2004. A world-wide study of high altitude treeline temperatures. J. Biogeogr. 31, 713–732. https://doi.org/10.1111/j.1365-2699.2003.01043.x.

Kuznetsova, A., Brockhoff, P.B., Christensen, R.H.B., 2017. lmerTest package: tests in linear mixed effects models. J. Stat. Softw. 82. https://doi.org/10.18637/jss.v082.i13.

Larsen, K.L., Barsberg, S., 2010. Theoretical and Raman spectroscopic studies of phenolic lignin model monomers. J. Phys. Chem. B 114, 8009–8021. https://doi.org/10.1021/jp1028239.

Li, L., Vrieling, A., Skidmore, A., Wang, T., Muñoz, A.R., Turak, E., 2015. Evaluation of MODIS spectral indices for monitoring hydrological dynamics of a small, seasonally-flooded wetland in southern Spain. Wetlands 35, 851–864. https://doi.org/10.1007/s13157-015-0676-9.

López-Blanco, E., Lund, M., Williams, M., Tamstorf, M.P., Westergaard-Nielsen, A., Exbrayat, J.-F., Hansen, B.U., Christensen, T.R., 2017. Exchange of $CO_2$ in Arctic tundra: impacts of meteorological variations and biological disturbance. Biogeosciences 14, 4467–4483. https://doi.org/10.5194/bg-14-4467-2017.

Lund, M., Raundrup, K., Westergaard-Nielsen, A., López-Blanco, E., Nymand, J., Aastrup, P., 2017. Larval outbreaks in West Greenland: instant and subsequent effects on tundra ecosystem productivity and $CO_2$ exchange. Ambio 46, 26–38. https://doi.org/10.1007/s13280-016-0863-9.

Lupoi, J.S., Gjersing, E., Davis, M.F., 2015. Evaluating lignocellulosic biomass, its derivatives, and downstream products with Raman spectroscopy. Front. Bioeng. Biotechnol. 3, 1–18. https://doi.org/10.3389/fbioe.2015.00050.

Moura, J.C.M.S., Bonine, C.A.V., de Oliveira Fernandes Viana, J., Dornelas, M.C., Mazzafera, P., 2010. Abiotic and biotic stresses and changes in the lignin content and composition in plants. J. Integr. Plant Biol. 52, 360–376. https://doi.org/10.1111/j.1744-7909.2010.00892.x.

Myburg, A.A., Lev-Yadun, S., Sederoff, R.R., 2013. Xylem structure and function. ELS. John Wiley & Sons, Ltd, Chichester, UK, pp. 1–9 https://doi.org/10.1002/9780470015902.a0001302.pub2 (& Sons, Ltd, Chichester, UK, pp. 1–9. doi:10.1038/npg.els.0001302).

Myers-Smith, I.H., Hik, D.S., 2018. Climate warming as a driver of tundra shrubline advance. J. Ecol. 106, 547–560. https://doi.org/10.1111/1365-2745.12817.

Myers-Smith, I.H., Forbes, B.C., Wilmking, M., Hallinger, M., Lantz, T., Blok, D., Tape, K.D., Macias-Fauria, M., Sass-Klaassen, U., Lévesque, E., Boudreau, S., Ropars, P., Hermanutz, L., Trant, A., Collier, L.S., Weijers, S., Rozema, J., Rayback, S.A., Schmidt, N.M., Schaepman-Strub, G., Wipf, S., Rixen, C., Ménard, C.B., Venn, S., Goetz, S., Andreu-Hayles, L., Elmendorf, S., Ravolainen, V., Welker, J., Grogan, P., Epstein, H.E., Hik, D.S., 2011. Shrub expansion in tundra ecosystems: dynamics, impacts and research priorities. Environ. Res. Lett. 6, 045509. https://doi.org/10.1088/1748-9326/6/4/045509.

Myers-Smith, I.H., Elmendorf, S.C., Beck, P.S.A., Wilmking, M., Hallinger, M., Blok, D., Tape, K.D., Rayback, S.A., Macias-Fauria, M., Forbes, B.C., Speed, J.D.M., Boulanger-Lapointe, N., Rixen, C., Lévesque, E., Schmidt, N.M., Baittinger, C., Trant, A.J., Hermanutz, L., Collier, L.S., Dawes, M.A., Lantz, T.C., Weijers, S., Jørgensen, R.H., Buchwal, A., Buras, A., Naito, A.T., Ravolainen, V., Schaepman-Strub, G., Wheeler, J.A., Wipf, S., Guay, K.C., Hik, D.S., Vellend, M., 2015. Climate sensitivity of shrub growth across the tundra biome. Nat. Clim. Chang. 5, 887–891. https://doi.org/10.1038/nclimate2697.

Parent, M.B., Verbyla, D., 2010. The Browning of Alaska's boreal Forest. Remote Sens. 2, 2729–2747. https://doi.org/10.3390/rs2122729.

Pinheiro, J.C., Bates, D.M., 2000. Linear mixed-effects models: Basic concepts and examples. Mixed-Effects Models in S and S-PLUS. Springer-Verlag, New York, pp. 3–56 https://doi.org/10.1007/0-387-22747-4_1.

Post, E., Pedersen, C., 2008. Opposing plant community responses to warming with and without herbivores. Proc. Natl. Acad. Sci. 105, 12353–12358. https://doi.org/10.1073/pnas.0802421105.

Prendin, A.L., Carrer, M., Karami, M., Hollesen, J., Bjerregaard Pedersen, N., Pividori, M., Treier, U.A., Westergaard-Nielsen, A., Elberling, B., Normand, S., 2020. Immediate and carry-over effects of insect outbreaks on vegetation growth in West Greenland assessed from cells to satellite. J. Biogeogr. 47, 87–100. https://doi.org/10.1111/jbi.13644.

Rathgeber, C.B.K., Cuny, H.E., Fonti, P., 2016. Biological basis of tree-ring formation: a crash course. Front. Plant Sci. 7, 734. https://doi.org/10.3389/fpls.2016.00734.

Schweingruber, F.H., 1996. Tree rings and environment Dendroecology. Paul Haupt Verlag, Berne, p. 609.

Seo, J., Jang, I., Jung, J.Y., Lee, Y.K., Kang, H., 2015. Warming and increased precipitation enhance phenol oxidase activity in soil while warming induces drought stress in vegetation of an Arctic ecosystem. Geoderma 259–260, 347–353. https://doi.org/10.1016/j.geoderma.2015.03.017.

Suseela, V., 2019. Potential roles of plant biochemistry in mediating ecosystem responses to warming and drought, ecosystem consequences of soil warming. Elsevier Inc https://doi.org/10.1016/B978-0-12-813493-1.00005.

Sutton, A., Tardif, J., 2005. Distribution and anatomical characteristics of white rings in Populus tremuloides. IAWA J. 26, 221–238.

Tape, K., Sturm, M., Racine, C., 2006. The evidence for shrub expansion in northern Alaska and the Pan-Arctic. Glob. Chang. Biol. 12, 686–702. https://doi.org/10.1111/j.1365-2486.2006.01128.x.

Tømmervik, H., Johansen, B., Tombre, I., Thannheiser, D., Høgda, K.A., Gaare, E., Wielgolaski, F.E., 2004. Vegetation changes in the nordic mountain birch forest: the influence of grazing and climate change. Arctic, Antarct. Alp. Res. 36, 323–332. https://doi.org/10.1657/1523-0430(2004)036[0323:VCITNM]2.0.CO;2.

Vibe, C., 1971. Lavere dyr i Grønland [Smaller animals in Greenland]. In: Böcher, T.W., Nielsen, C.O., Schou, A. (Eds.), Danmarks Natur. Politikens Forlag, Copenhagen, pp. 444–452.

Villari, C., Faccoli, M., Battisti, A., Bonello, P., Marini, L., 2014. Testing phenotypic trade-offs in the chemical defence strategy of scots pine under growth-limiting field conditions. Tree Physiol. 34, 919–930. https://doi.org/10.1093/treephys/tpu063.

Voelker, S.L., Lachenbruch, B., Meinzer, F.C., Kitin, P., Strauss, S.H., 2011. Transgenic poplars with reduced lignin show impaired xylem conductivity, growth efficiency and survival. Plant Cell Environ. 34, 655–668. https://doi.org/10.1111/j.1365-3040.2010.02270.x.

War, A.R., Paulraj, M.G., Ahmad, T., Ahad, A., Hussain, B., Ignacimuthu, S., Sharma, H.C., War, A.R., Paulraj, M.G., Ahmad, T., Buhroo, A.A., Hussain, B., Ignacimuthu, S., Sharma, H.C., 2012. Mechanisms of plant defense against insect herbivores. Plant Signal. Behav. 7 (10), 1306–1320. https://doi.org/10.4161/psb.21663.

Westergaard-Nielsen, A., Karami, M., Hansen, B.U., Westermann, S., Elberling, B., 2018. Contrasting temperature trends across the ice-free part of Greenland. Sci. Rep. 8, 1586. https://doi.org/10.1038/s41598-018-19992-w.

Wiley, J.H., Atalla, R.H., 1987. Band assignments in the Raman spectra of celluloses. Carbohydr. Res. 160.

Wilmking, M., Buras, A., Lehejček, J., Lange, J., Shetti, R., van der Maaten, E., 2018. Influence of larval outbreaks on the climate reconstruction potential of an Arctic shrub. Dendrochronologia 49, 36–43. https://doi.org/10.1016/j.dendro.2018.02.010.

Xu, F., Sun, R.C., Lu, Q., Jones, G.L., 2006. Comparative study of anatomy and lignin distribution in normal and tension wood of *Salix gordejecii*. Wood Sci. Technol. 40, 358–370. https://doi.org/10.1007/s00226-005-0049-2.

Young, A.B., Watts, D.A., Taylor, A.H., Post, E., 2016. Dendrochronologia species and site differences influence climate-shrub growth responses in West Greenland. Dendrochronologia 37, 69–78. https://doi.org/10.1016/j.dendro.2015.12.007.

Zar, J.H., 1999. Biostatistical analysis fifth edition. USA Prentice Hall 4165, 4159–4165.

Zuur, A.F., Ieno, E.N., Walker, N., Saveliev, A.A., Smith, G.M., 2009. Mixed effects models and extensions in ecology with R. Statistics for Biology and Health. Springer New York, New York, NY https://doi.org/10.1007/978-0-387-87458-6.